Selective fiber Bragg grating inscription in four-core fiber for two-dimension vector bending sensing

WEIJIA BAO,[1,2] NAMITA SAHOO,[2] ZHONGYUAN SUN,[1,2] CHANGLE WANG,[2] SHEN LIU,[1,2,*] YIPING WANG,[1,3] AND LIN ZHANG[2]

[1] *Key Laboratory of Optoelectronic Devices and Systems of Ministry of Education and Guangdong Province, College of Optoelectronic Engineering, Shenzhen University, Shenzhen 518060, China*
[2] *Aston Institute of Photonic Technologies, Aston University, Birmingham B4 7ET, UK*
[3] *Shenzhen Photonic Sensing Technology Co., Ltd., China*
[*]shenliu@szu.edu.cn

Abstract: The paper presents selective fiber Bragg grating (FBG) inscription in four-core fiber based on a phase mask scanning method. The inscription factors are systematically investigated, which involves fiber core position and focused laser beam size in fiber, etc. Several specific inscriptions (including individual, dual and all inscriptions) are demonstrated. Two orthogonally positioned cores are selectively inscribed and applied to two-dimension vector bending measurement. The measured bending sensitivities of two FBGs range from -54.3 pm/m^{-1} to 52.2 pm/m^{-1} and -53.7 pm/m^{-1} to 52.8 pm/m^{-1}, respectively. More importantly, it has been revealed that their sensitivities versus bending direction follow regular cosinoidal and sinusoidal distribution. The direction and amplitude of the vector bending can be recovered using measured central wavelength shifts of those two FBGs.

1. Introduction

Recent years, various multi-core fiber (MCF) devices are proposed, improving the light propagation, transmission capacity and multiplexing features. MCF devices have contributed to the development of optical fiber communication [1–2], fiber laser [3–4], and fiber sensing [5–8]. As the classic fiber device, fiber Bragg gratings (FBGs) have also been developed in MCF [9–13] for the further application of these mentioned fields. Especially in the field of fiber sensing, diverse directional bending sensors based on MCF-FBG have been successfully investigated [14–18]. These bending sensors can respond not just to the magnitude but also the direction because the spatial positions of the different cores produce a differential strain distribution in the transversal cross section when the fiber is bent. So they can provide sufficient information about both bending magnitude and direction, which is significant for some engineering applications, like structure health monitoring and smart robotic arm. However, in most previous reports, the FBGs are simultaneously inscribed in all cores of MCF [9,14,16–18]. The Bragg wavelengths of FBGs in each core are slightly different due to the lens effect [19] of the fiber cladding, resulting in inconsistent effective refractive index modulation on fiber cores. In addition, the cores of MCF are not always axially parallel and straight, so they might be twisted and helically distributed in a certain length. The randomly positioned fiber cores could cause the FBG inhomogeneity, further sacrificing the consistency and properties of sensor in practice. Therefore, sweeping FBG inscription in all cores of MCF has some limitations in itself, thus the selective FBG inscription is quite necessary.

For the selective inscription, the key lies in the control of core positioning and laser exposure. As reported in Ref. [20], selective inscription is easily realized by adjusting the spatial fiber core position, which has good accuracy and repeatability. But only long period grating is

implemented by this method due to that the FBG inscription requires high exposure accuracy. With an optimized setup, different inscriptions are feasible via carefully adjusting both the the laser beam size and the spatial distance between the fiber and the phase mask [21]. They can fabricate gratings in individual core and multi cores of seven core fiber. It has a high requirement on the focused laser in fiber because the laser can radiate in other unselected cores with high exposure power and inaccurate focused laser position and further result in grating formation. In contrast, we present a relatively easy-assembly selective inscription via spatial fiber core positioning and focused laser adjusting in our previous work [22]. The flexibility and feasibility of selective inscription are improved. But the core position could be twisted when moving the fiber before the inscription. So the repeatability of that selective inscription is still unsatisfactory.

In the work reported here, we have proposed and experimentally demonstrated the selective fiber Bragg grating inscription in four-core fiber (FCF) for two-dimension vector bending sensing. Aiming at solving the limitation of selective inscription of MCF, we improve the FBG inscription process. The selective inscription is accomplished by the modified ultraviolet laser based fabrication and fiber core positioning method. The influence of FBG-formation factors is systematically studied. The positioning methods are broadly appropriate for the selective inscription of various multi core fibers (MCFs), which make good sense for the MCF grating inscription. Moreover, the bending induced stress variation in fiber is simulated in order to explain the vector bending sensing feasibility of FBG in FCF. Finally, the bending sensing performance of the inscribed FBGs in FCF is analyzed in detail. The sensor can directly measure two orthogonal principal components of two-dimension bending vector, and the magnitude and direction of original bending can be identified via simple trigonometric analysis.

2. Selective inscription

As shown in Fig. 1(a), the fiber we used is FCF whose cores are highly photosensitive (Germanium and Boron co-doped) and arranged in the corners of a 50-μm-side square lattice. The diameters of its cladding and core are 125 μm and 8 μm, respectively. In the fabrication, the grating is inscribed by the phase mask scanning method using an argon ion frequency-doubled 244 nm laser. In order to achieve selective FBG inscription in FCF, we proposed two methods of fiber core positioning for positioning fiber cores against the UV beam, and the adjustment of focused laser area for core inscription. The detailed fabrication of FCF-FBG is presented in the following.
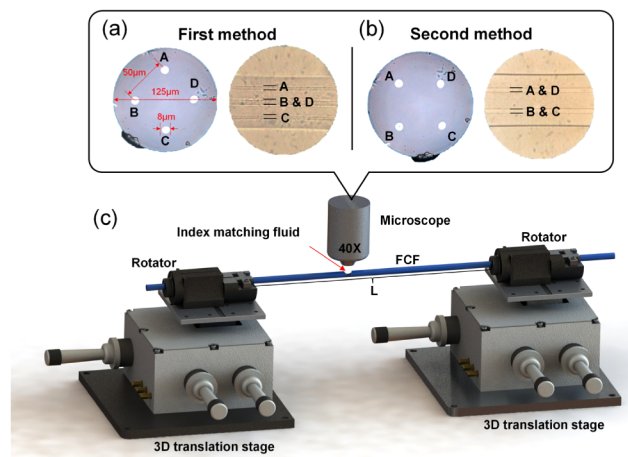
Fig. 1. Schematic diagram of selective inscription: microscopic images of FCF from (a) cross-section view and (b) lateral view; (c) setup of core positioning.

2.1. Fiber core positioning

The selective inscription is mainly based on the fiber core positioning. Here, the core position could be changed when moving the fiber to the inscription stage. So we set up the microscope over the the inscription stage for fiber positioning. The core position remains unchanged after positioning, which will eliminate the unexpected problems induced by moving fiber. As shown in Fig. 1(c), the FCF (total length of 20 cm) was fixed between two rotators that were mounted on three-dimensional (3D) translation stages. The spatial position of fiber cores can be determined and optionally adjusted under microscope by the rotators and stages. The core position can be observed through the microscope (magnification of 40 times). We positioned the fiber core position for two different geometric distributions by rotating the FCF, see Figs. 1(a) and 1(b). In detail, from the cross-section view, the core position presents rhombus and square distribution in two cases, respectively. While from the lateral view, the cores present the patterns of three parallel lines and two parallel lines because the images of cores that have the same lateral view are overlapped, such as cores of B and D in Fig. 1(a) or cores of A and D, B and C in Fig. 1(b). Under different core distribution conditions, different selective inscriptions (including simultaneous inscription of all cores, and individual or dual cores) can be achieved according to the design.

2.2. Grating inscription

The inscription process is shown in Fig. 2(a), the laser is focused by the cylindrical lens and then through the phase mask (Ibsen Ltd). In the conventional FBG inscription, the laser beam is focused in the fiber core center and the beam size is fixed. By contrast, the effective laser beam size and position focused in fiber will be adjusted by the relative height and defocusing length between fiber and laser beam for selective inscription. Generally, the effective laser beam size before cylindrical lens is approximately 450 μm measured by a UV beam profiler and it can be focused to around 22 μm at the focus point (the fiber is fixed 87 mm away from the lens). FBG formation in fiber core is determined by the laser exposure. Hence, it is important to control the exposure area inside fiber. It is clearly observed that the exposure area in fiber of the focused laser is larger than that of the defocused laser, as shown in Figs. 2(b) and 2(c). The single FBG inscription in FCF is aimed for a selected core, thus the laser can effectively focused into the specified core and avoid other unselected core areas. But for the multi-FBG inscription, the laser beam size is slightly defocused to cover all cores.

The FBG inscription was performed with laser output power of 30 mW and a scanning velocity of 0.10 mm/s over 5.0 mm length. The fan-in/out coupler was spliced to the one end of the FCF for monitoring the FBG reflection from individual core. Under the first positioning condition, we can realize three different FBG inscriptions according to our needs: single-core, dual-core and all-core inscription. In the single-core inscription, the relative height change between fiber and laser can be estimated by observing the laser diffraction pattern after it passes through the fiber [23,24]. The laser was intentionally focused on core A. Because the laser beam size is small, the UV exposure will only introduce FBG structure in core A not others. Figure 3(a) shows the spectra of all 4 cores, but only one strong reflection resonance with central wavelength of 1551.72 nm occurred in core A, and the remaining three cores show almost no FBG reflection. Notably, there is a weak reflection peak on core B spectrum. Although the laser is focused in core A, core B can also be irradiated by laser because the laser beam size is relatively big at defocused position. So laser might exposure to core B, an unexpected FBG is inscribed in core B. But it is absolutely avoidable with controlling focused laser position in fiber. Therefore, the proposed single-core inscription is effective. In the dual-core inscription, the laser was focused on to the fiber center, thus both of core B and D were irradiated by the slightly defocused laser. As shown in Fig. 3(b), we can see two reflection resonances were obtained for the dual-core inscription. Here, the laser reaches core B first before core D, resulting in weakened refractive-index modulation on core D. So the FBG in core D produced a weaker reflection, in contrast to the FBG in core B.
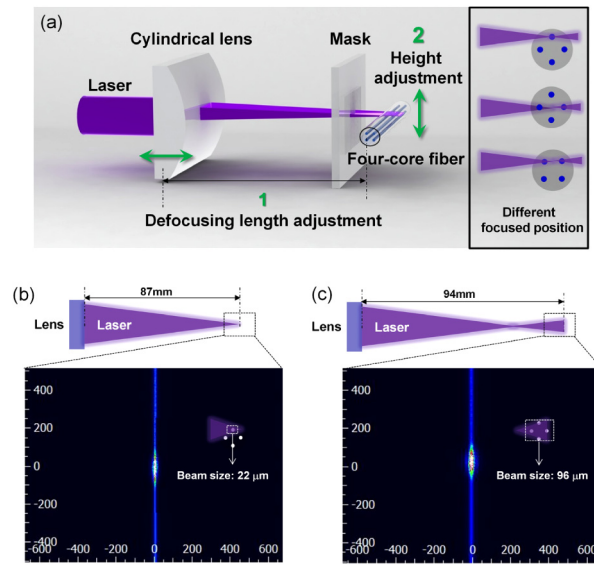
Fig. 2. (a) Schematic diagram of FBG inscription in a FCF (insert: different focused position), (b) image of UV beam at focused point; (c) image of UV beam at defocused point.

Finally in the all-core inscription, in order to inscribe FBGs in all cores, the cylindrical lens was
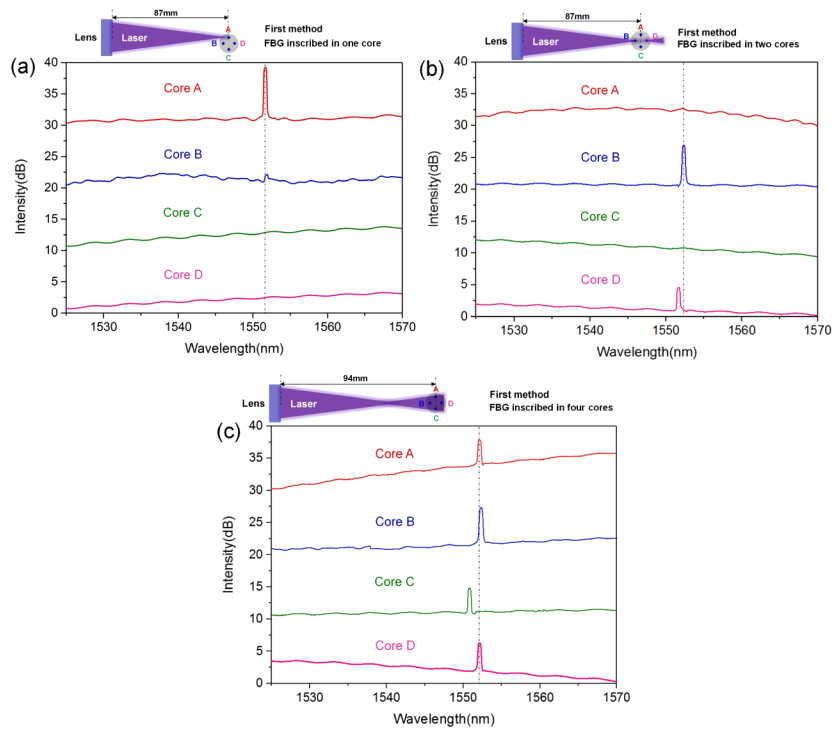
Fig. 3. Spectra of (a) single-core FBG inscription, (b) dual-core FBG inscription and (c) all-core FBG inscription.

set to be 94 mm away from the FCF center, the laser beam size was increased from 22 μm to 96 μm in the fiber position to cover all 4 cores. As shown in Fig. 3(c), we clearly see each core exhibits a reflection resonance around 1552 nm.

Under the second FCF positioning condition, we can realize two different FBG inscriptions according to our needs: dual-core and all-core inscription. The inscriptions were accomplished according to the similar procedure. For the dual-core inscription, the focused laser was adjusted to the upper area of core A and D position, then FBGs were inscribed in the core A and D with FBG in the former slightly stronger than that in the latter, as shown in Fig. 4(a). For the all-core inscription, the cylindrical lens was moved to the defocused position (94 mm away from the FCF center) aiming to cover all 4 cores. As shown in Fig. 4(b), all 4 cores show Bragg reflections with similar strength but slightly different central wavelength, which can be attributed to the fact that effective refractive index of each core is not identical due to the laser power fluctuation on different cores. Ideally, the FBG inscribed under the same condition should be identical. However, the effective refractive index value of each core is not consistent, which is caused by slightly different doping concentration or residual stress. Therefore, the cores inscribed under the same condition will show different reflections, such as core A and C of all-core inscription with the first method, or core A and B of all-core inscription with the second method.
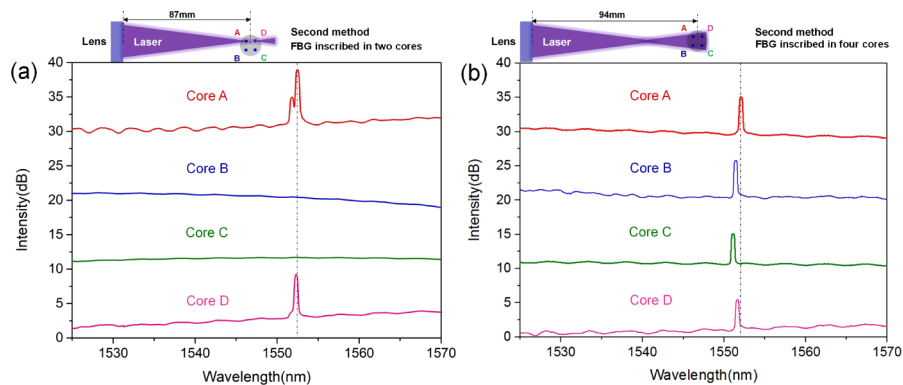

Fig. 4. Spectrum of (a) dual-core FBG inscription; (b) all-core FBG inscription.

3. Vector sensing mechanism

The optical fiber can be equivalent to a cantilever beam, the effect of stress on the bent FCF can be analyzed by the finite element analysis of ANSYS. For the simulation using ANSYS, we set the fiber cantilever beam with a length of 100 mm and diameter of 120 μm, and the radius of curvature due to bending is 250 mm. For the convenience in analyzing the fiber cantilever beam, we set up the bending direction is along the positive y-axis. As shown in Figs. 5(a) and 5(b), the stress distribution is gradually changed along the bending direction (positive y-axis), but constant at the direction normal to the bending (x-axis). The stretching stress is gradually translated to compressive stress along the positive y-axis. Therefore, the fiber bending induced stress effects on two orthogonal axes are independent. The arbitrary bending vector in two-dimensional plane can be decomposed into two orthogonal components, so the bending vector can be recovered by two individual component measurements, as shown in Fig. 5(c): the vector projection in the x-axis and the projection in y-axis. The sensor that has orthogonal-positioned components is perfect for vector bending measurement. The cores of FCF are pairwise orthogonal, which provides two intrinsic orthogonal sensing elements. Thus, the FCF device can be a vector bent

sensor by directly detecting two orthogonal principal components of bending if we integrated two sensing elements into a section of FCF via selective FBG inscriptions, as shown in Fig. 5(d).
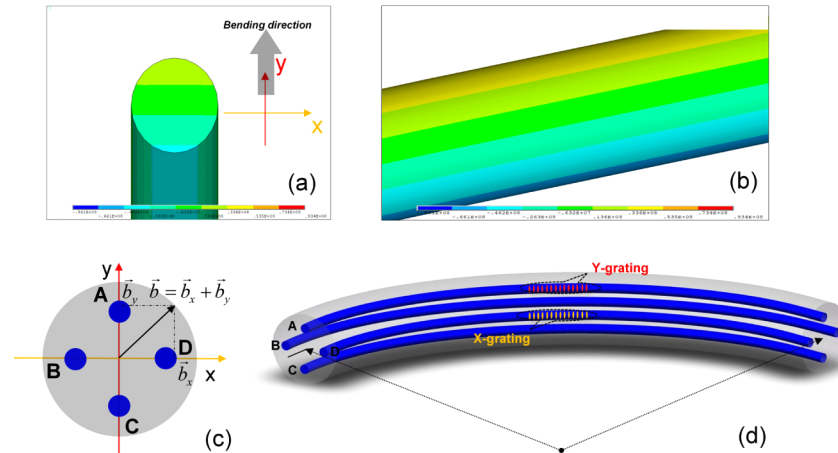

Fig. 5. (a) Stress variation of fiber cross-section, (b) stress variation of fiber lateral, (c) diagram of vector decomposition, (d) schematic diagram of two-component FBG in FCF.

4. Measurement and discussion

To accomplish an orthogonal two-component sensing configuration, two FBGs were selectively inscribed into core A and D via the single-core inscription using the first FCF positioning method. The FBGs in the two cores were intentionally inscribed at two different wavelengths (A: at 1540.87 nm; B: at 1560.62 nm) for the discriminating measurement for the two components. Assuming that core A and D are located at two orthogonal axes (y-axis and x-axis) of two-dimensional bending plane. For clarity, the FBGs inscribed into core A and D are named y-grating and x-grating, respectively. Those two FBGs will be utilized to respond to bending components in different directions. The experimental setup of Fig. 1(c) is used to investigate response of the FCF FBGs for directional bending sensing. Because both sides of the device are fixed, the fiber is under bent when moving the one stage toward another one. And the change of bending direction is achieved by rotating the FCF using the rotator.

The applied bending curvature C can be calculated by [25]: $\sin\left(\frac{LC}{2}\right) = \frac{(L-\Delta L)}{2}C$. Where L is the initial separation distance between the two fixed ends of the straight FCF, ΔL represents the displacement of the stage. As discussed in section 3, each core will be stretched or compressed when FCF is bent along its coordinate axis, resulting in the increase or decrease of FBG period. So the period variation will induce a corresponding wavelength shift in spectrum response. However, any core will not be significantly affected when applied bending direction is normal to its coordinate axis because it is located at neutral axis of fiber, which makes it insensitive along that bending direction. The x-grating and y-grating are orthogonally positioned, they will have mutually-independent responses to bending in each direction, providing a mechanism for vector sensing. The measurement for directional responses was firstly conducted for verifying above analysis. Applying a certain curvature to the FCF, the bending direction is changed at step-wise (with a rotation step of 30°). The wavelength responses of x-grating and y-grating to bending direction show analogously sinusoidal and cosinoidal distribution over a full range of 0-360°, respectively, as the results shown in Figs. 6(a) and 6(b). Responses of x-grating and y-grating are mutually independent but both execute component sensing responsibilities. That means the drawback of one FBG in certain direction can be compensated by another one. In the event that

the sensitivity of one FBG in initial direction is low, we can obtain the information of magnitude via referring to measured result of other one because their sensitivity distributions are opposite to each other. Thus, based on the sensing mechanism discussed above, the applied bending direction can be recovered via monitoring wavelength responses of x-grating and y-grating.
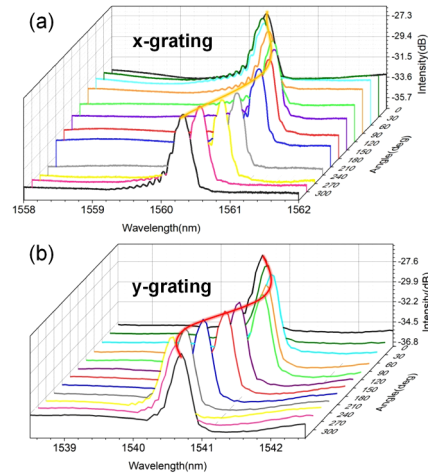

Fig. 6. (a) Spectral responses of x-grating, (b) spectral responses of y-grating.

The bending sensitivities for different directions were also measured for further verifying the performance of those two FBGs in FCF. The bending was applied to the FCF at different directions, and we plot the central wavelengths of two FBGs as a function of the bending curvature at four specific bending directions: 0°, 90°, 180° and 270°. As shown in Figs. 7(a) and 7(b), x-grating is most sensitive along x-axis (0° and 180°), the curvature sensitivities are −54.3 pm/m^{-1} and 52.2 pm/m^{-1}, respectively. But y-grating shows an opposite trends, as it is most sensitive along y-axis (90° and 270°), and the curvature sensitivities are 52.8 pm/m^{-1} and −53.7 pm/m^{-1}, respectively. These results clearly show that the FCF-FBG have no obvious response when the bending direction is normal to its own axis. The full direction dependence of bending sensitivity was also measured as the FCF was rotated from 0° to 360° with a rotating step of 30°, the experimental results are shown in Fig. 8.
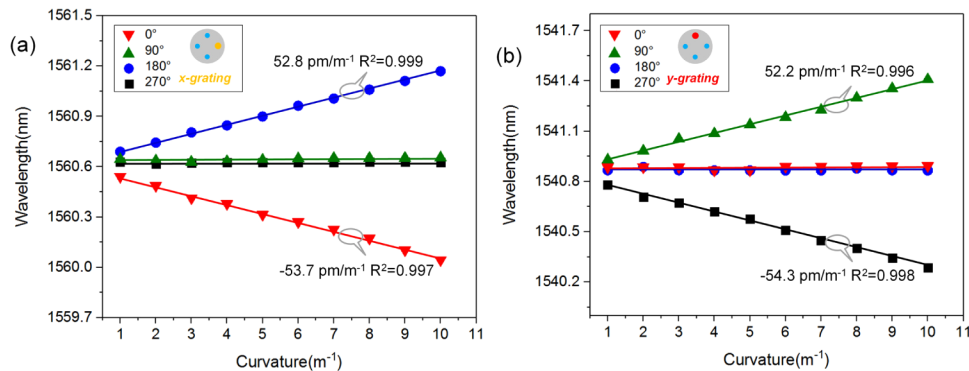
Fig. 7. Linear responses versus increasing curvature in different direction of (a) x-grating, (b) y-grating.
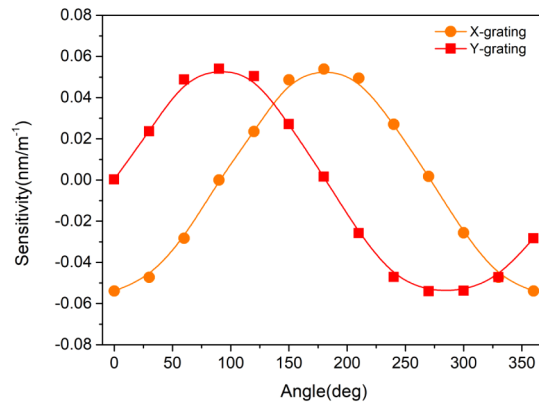
Fig. 8. Sensitivities of x-grating and y-grating in an FCF versus bending direction from 0° to 360°.

The sensitivity distributions of x-grating and y-grating follow approximate cosine and sine function, i.e. $b_x cos(\theta)$ and $b_x sin(\theta)$, (b is the curve amplitude of bending sensitivity distributions, θ is bending direction). With the same measuring operation of each FBG, fiber bending can result in different wavelength modulation on the Bragg wavelength of the x and y-grating in different direction. Thus the wavelength responses of two FBGs can be utilized to synthesize a full vector bending (by means of trigonometric calculation), effectively monitoring the curvature and direction when a structure is under bending.

5.   Conclusions

In conclusion, we have achieved the selective FBG inscriptions in FCF. The effect of the geometrical arrangement of cores, defocus length and the relative position between laser beam and fiber cores are studied. Two FBGs are inscribed in two orthogonal-positioned cores of FCF based on the selective inscription. Taking advantage of the regular cosinoidal and sinusoidal central wavelength responses to two-dimensional vector bending, the FCF-FBG device can be utilized to analyze the curvature and direction of fiber bending simultaneously. From an application point of view, the highly compact sensing configuration and great direction dependence make FCF-FBGs as ideal vector sensor for applications of mechanical engineering and robotic arm that requires the real-time direction identification and critical resistance to electromagnetic interference. Also the selective FBG inscription in FCF is useful for some other sensing measurements, fiber communications and lasers, which will be the focus of our future work.

Disclosures

The authors declare no conflicts of interest.

References

1. P. J. Winzer and C. R. Doerr, "Multi-core optical fiber and optical communication systems," United States Patent, **US 8,503,845 B2**, (2013).
2. R. J. Essiambre, R. Ryf, N. K. Fontaine, and S. Randel, "Breakthroughs in Photonics 2012: Space-Division Multiplexing in Multimode and Multicore Fibres for High-Capacity Optical Communication," IEEE Photonics J. **5**(2), 0701307 (2013).
3. C. Jollivet, A. Mafi, D. Flamm, M. Duparré, K. Schuster, S. Grimm, and A. Schülzgen, "Mode-resolved gain analysis and lasing in multi-supermode multi-core fiber laser," Opt. Express **22**(24), 30377–30386 (2014).
4. Y. B. Zheng, J. Q. Yao, L. Zhang, Y. Wang, W. Q. Wen, R. Zhou, Z. G. Di, and L. Jing, "Supermode analysis in multi-core photonic crystal fiber laser," Proc. SPIE **7843**, 784316 (2010).
5. J. P. Moore and M. D. Rogge, "Shape sensing using multi-core fibre optic cable and parametric curve solutions," Opt. Express **20**(3), 2967–2973 (2012).
6. G. Salceda-Delgado, A. V. Newkirk, J. E. Antonio-Lopez, A. Martinez-Rios, A. Schülzgen, and R. A. Correa, "Compact fiber-optic curvature sensor based on super-mode interference in a seven-core fiber," Opt. Lett. **40**(7), 1468–1471 (2015).
7. M. Amanzadeha, S. M. Aminossadatia, M. S. Kizila, and A. D. Rakić, "Recent developments in fibre optic shape sensing," Measurement **128**, 119–137 (2018).
8. S. X. Zhang, A. Zhou, H. Y. Guo, Y. J. Zhao, and L. B. Yuan, "Highly sensitive vector curvature sensor based on a triple-core fiber interferometer," OSA Continuum **2**(6), 1953–1963 (2019).
9. P. S. Westbrook, T. Kremp, K. S. Feder, W. Ko, E. M. Monberg, H. C. Wu, D. A. Simoff, T. F. Taunay, and R. M. Ortiz, "Continuous Multicore Optical Fiber Grating Arrays for Distributed Sensing Applications," J. Lightwave Technol. **35**(6), 1248–1252 (2017).
10. A. Donko, M. Beresna, Y. Jung, J. Hayes, D. J. Richardson, and G. Brambilla, "Point-by-point femtosecond laser microprocessing of independent core-specific fiber Bragg gratings in a multi-core fiber," Opt. Express **26**(2), 2039–2044 (2018).
11. Y. S. Zhang, W. G. Zhang, Y. X. Zhang, S. Wang, L. Yu, and Y. Y. Yan, "Simultaneous measurement of curvature and temperature based on LP_{11} mode Bragg grating in seven-core fiber," Meas. Sci. Technol. **28**(5), 055101 (2017).
12. Y. Zou, X. P. Dong, G. B. Lin, and R. Adhami, "Wide Range FBG Displacement Sensor Based on Twin-Core Fiber Filter," J. Lightwave Technol. **30**(3), 337–343 (2012).
13. K. Bronnikov, A. Wolf, S. Yakushin, A. Dostovalov, O. Egorova, S. Zhuravlev, S. Semjonov, S. Wabnitz, and S. Babin, "Durable shape sensor based on FBG array inscribed in polyimide-coated multicore optical fiber," Opt. Express **27**(26), 38421–38434 (2019).
14. D. Barrera, J. Madrigal, S. Delepine-Lesoille, and S. Sales, "Multicore optical fiber shape sensors suitable for use under gamma radiation," Opt. Express **27**(20), 29026–29033 (2019).
15. K. M. Yang, J. He, C. R. Liao, Y. Wang, S. Liu, K. K. Guo, J. T. Zhou, Z. Y. Li, Z. Tan, and Y. P. Wang, "Femtosecond Laser Inscription of Fiber Bragg Grating in Twin-core Few-mode Fiber for Directional Bend Sensing," J. Lightwave Technol. **35**(21), 4670–4676 (2017).
16. M. X. Hou, K. M. Yang, J. He, X. Z. Xu, S. Ju, K. K. Guo, and Y. P. Wang, "Two-dimensional vector bending sensor based on seven-core fiber Bragg gratings," Opt. Express **26**(18), 23770–23781 (2018).
17. D. Zheng, J. Madrigal, H. L. Chen, D. Barrera, and S. Sales, "Multicore fiber-Bragg-grating-based directional curvature sensor interrogated by a broadband source with a sinusoidal spectrum," Opt. Lett. **42**(18), 3710–3713 (2017).
18. H. L. Zhang, Z. F. Wu, P. Shum, R. X. Wang, X. Q. Dinh, S. N. Fu, W. J. Tong, and M. Tang, "Fiber Bragg gratings in heterogeneous multicore fiber for directional bending sensing," J. Opt. **18**(8), 085705 (2016).
19. C. Hnatovsky, D. Grobnic, and S. J. Mihailov, "Nonlinear photoluminescence imaging applied to femtosecond laser manufacturing of fiber Bragg gratings," Opt. Express **25**(13), 14247–14259 (2017).
20. D. Barrera, J. Madrigal, and S. Sales, "Long Period Gratings in Multicore Optical Fibers for Directional Curvature Sensor Implementation," J. Lightwave Technol. **36**(4), 1063–1068 (2018).
21. I. Gasulla, D. Barrera, J. Hervás, and S. Sales, "Spatial Division Multiplexed Microwave Signal processing by selective grating inscription in homogeneous multicore fibers," Sci. Rep. **7**(1), 41727 (2017).
22. C. L. Wang, Z. J. Yan, Q. Z. Sun, Z. Y. Sun, C. B. Mou, J. X. Zhang, A. Badmos, and L. Zhang, "Fibre Bragg gratings fabrication in four core fibres," Proc. SPIE **9886**, 98860H (2016).
23. D. Y. Feng, X. G. Qiao, and J. Albert, "Off-axis ultraviolet-written fiber Bragg gratings for directional bending measurements," Opt. Lett. **41**(6), 1201–1204 (2016).
24. W. J. Bao, Q. Z. Rong, F. Y. Chen, and X. G. Qiao, "All-fiber 3D vector displacement (bending) sensor based on an eccentric FBG," Opt. Express **26**(7), 8619–8627 (2018).
25. W. J. Zhou, Y. Zhou, X. Y. Dong, L. Y. Shao, J. Cheng, and J. Albert, "Fiber-Optic Curvature Sensor Based on Cladding-Mode Bragg Grating Excited by Fiber Multimode Interferometer," IEEE Photonics J. **4**(3), 1051–1057 (2012).